Nonlocal Hydrodynamic Theory of Flow in Polymer Layers

David T. Wu*,†,‡ and M. E. Cates‡,§

Department of Chemical Engineering, University of California, Santa Barbara, California 93106, Department of Physics and Astronomy, University of Edinburgh, JCMB, King's Buildings, Mayfield Road, Edinburgh EH9 3JZ, U.K., and Cavendish Laboratory, Madingley Road, Cambridge CB3 0HE, U.K.

Received December 14, 1995[⊗]

ABSTRACT: We present a nonlocal hydrodynamic theory for flow through an adsorbed layer of homopolymer. Our theory is based upon a multiple-scattering treatment in which the polymer is decomposed into loops, each attached to the surface at a point and obeying Zimm dynamics. The multiple scattering series is converted into an integral equation which we solve numerically. The dependence of our results on the truncation procedure in the sum over Zimm modes is discussed. Unlike previous models, which rely on a local porosity description, our theory explicitly incorporates polymer dynamics and is hence applicable to finite frequencies and (in principle) nonlinear responses. For an isolated layer, we present results for weak oscillatory and steady shear flows at Θ conditions. We also give results for steady flow between a pair of parallel plates coated with homopolymer, which may be relevant to the dynamics of polymer-coated colloids undergoing hydrodynamic collisions.

1. Introduction

Adsorbed polymer layers are of substantial interest to scientists and engineers, largely because of their central role in colloidal stabilization.[1,2] The understanding of such layers under flow conditions is important in several areas, e.g., flow between surfaces (lubrication, flow in capillary tubes), flow in porous media (filtration), and transport and rheology of polymer-stabilized colloidal suspensions. In the last case, it is very often the stability of a colloid under flow conditions (for example, in a mixing tank) that matters, rather than the purely thermodynamic stability which would be appropriate in the absence of flow. Crudely one can estimate the flow stability by comparing the magnitude of thermodynamic and hydrodynamic forces;[1] however, this neglects the fact that the fluid and the polymer interact directly with one another, so that additivity cannot be assumed. Also, such arguments do not allow for the finite dynamical response times of polymer chains.[3,4]

In fact, although much is now known about the structure of adsorbed homopolymer on surfaces, there is little detailed understanding of the behavior of these same systems subjected to flow. Previous models of the local fluid motion rely on a Darcy flow approximation, where the permeability is a (ad-hoc) function of the local segment density. The polymer is effectively regarded as a static porous medium with the same density profile as the original polymer layer. Models based on this type of description neglect the nonlocal response due to hydrodynamic coupling of the polymer to the fluid. If a section of polymer is subjected to a drag force, this propagates along the chain as a change in shape which exerts forces elsewhere on the fluid. Nonlocal hydrodynamic effects are known to be dominant in the dynamics of isolated polymer coils, and we expect them to play an important role also in the adsorbed layer problem.

Our approach to the problem of adsorbed layer rheology sets out to calculate the hydrodynamic response of the polymers to the flow and, conversely, of the flow profile to the polymer distribution. Some preliminary results were presented in ref 5 and (for grafted monodisperse loops) in ref 6. The present work gives full details of the method, and reports several extensions and checks. We include a careful examination of the convergence behavior with the number of modes used to describe a chain; the numerical results presented below differ in detail from those previously reported due to improved accuracy in this respect. Our method involves a multiple-scattering formalism based on the work of Freed and Edwards[7] for polymer solutions. That formalism reproduces the well-known results of the Zimm model[8] but, unlike simpler treatments, has a natural (if algebraically complicated) extension to cases where translational invariance cannot be assumed. To make progress, we have had to simplify and restrict the calculations in several ways.

Firstly, we represent the adsorbed homopolymers as a collection of loops, each attached to the adsorbing surface at a single point. (The role of tails is studied later.) By choosing a power law distribution of loop sizes,[9] it is possible to mimic rather accurately the structure expected in a real layer.

Secondly, for most of our calculations, we treat the adsorbing wall as penetrable both to the polymers and to fluid flow. This assumption is not important, however, since the high polymer density at the adsorbing wall itself leads to the formation of an impenetrable screen on which fluid motion (and hence, within our model, polymer motion) is frozen. This is checked explicitly in section 4.

Thirdly, we use Gaussian loops to model the adsorbed layer, which we assume to consist of chains at the Θ temperature, in which three-body interactions dominate. This model, in three dimensions, gives a self-similar density profile[10] in which polymer loops of any given size are close to the overlap threshold with each other. This geometrical feature is shared by the adsorbed layer of swollen chains for which a Gaussian model would, however, be less appropriate. Therefore, we believe that our results, although restricted, yield

* To whom correspondence should be addressed at the University of California.
† University of California.
‡ Cavendish Laboratory.
§ University of Edinburgh.
⊗ Abstract published in *Advance ACS Abstracts,* May 1, 1996.

S0024-9297(95)01845-6 CCC: $12.00

insight into the general case of adsorbed homopolymer.

Fourthly, on the basis of this geometrical picture, we allow for the Zimm dynamics of individual loops, but ignore screening corrections which, for dense polymer solutions, cause a crossover to Rouse-like behavior.[7] Such corrections should have only marginal effects in the layer since loops on a given scale are weakly interpenetrating. (In fact, if they were strongly interpenetrating, the loops would be entangled in a way that the Freed−Edwards theory cannot encompass.)

Finally, for numerical work we restrict our attention to the regime of linear response, in which the perturbation to the fluid motion from the presence of polymer can be calculated without accounting for the change in density profile of the chains arising in turn from the fluid motion itself. In principle, a nonlinear calculation is possible using our methods, and below we indicate how this should be done. However, such calculations in general require a self-consistent iteration loop which is prohibitive with present computer resources, and we do not pursue them here. (Recently a qualitative scaling approach has been developed which may be able to make some predictions in this nonlinear regime; see e.g. ref 11.)

The rest of this paper is organized as follows: In section 2 we describe the static decomposition of an adsorbed homopolymer layer into a polydisperse "pseudobrush" of grafted loops. Section 3 describes the multiple scattering formalism used for the dynamic problem, and outlines our numerical procedure for calculating the perturbed fluid velocity in the presence of adsorbed polymer. In sections 4 and 5 we give a selection of results, both for a single plate problem and for the flow in a channel between two polymer-coated plates. Section 6 contains a brief conclusion; various algebraic technicalities are relegated to the Appendix.

2. Statics: Loop Decomposition of a Polymer Layer

A layer of adsorbed homopolymer can be decomposed into trains of attachment, loops between the trains, and tails which, like loops, protrude from the surface.[2] We address the issue of tails in section 3d, but for simplicity we consider for the moment the layer to be composed of loops alone. This should be valid in the middle part of a layer consisting of high molecular weight chains. Furthermore, since trains lie flat against the wall, the hydrodynamically active part of such a polymer layer is a collection of loops. (A loop is considered to be the stretch of polymer between two attached adsorption points of the polymer.) The structure, and in particular the density profile, of the polymer layer is determined by the loop length distribution. In this way, a homopolymer layer can be treated as a very polydisperse pseudobrush of loops, in which loops of a given size only marginally overlap (close to the "mushroom" regime).[9]

The loop size distribution can be inferred from a knowledge of the segment density profile. In particular, when the monomer density profile as a function of height from the surface, $\phi(z)$, is given by the power law

$$\phi(z) \approx z^{-\alpha} \tag{1}$$

(which applies for weak adsorption, in either good or Θ conditions), the loop size distribution is then

$$P(L) = \rho L^{-\tau} \tag{2}$$

where the prefactor ρ is a constant with units of loops per unit surface area and the loop exponent τ is given by

$$\tau = 2 + \nu(\alpha - 1) \tag{3}$$

Here L is the loop contour length, and ν is the usual size exponent for loops (1/2 for Θ conditions, 3/5 for good solvent conditions). The amplitude of the power law under conditions of weak adsorption is independent of the bulk concentration. Instead, within a self-consistent field calculation,[12] the density profile in the central region is

$$\phi(z) = \frac{1}{3\nu}(z/a)^{-2} \tag{4}$$

for good solvent and

$$\phi(z) = (1/8w)^{1/2}(z/a)^{-1} \tag{5}$$

for Θ conditions. We can see that the amplitude is a function only of the excluded volume parameter, ν, in the first case, or only of the three-body interaction parameter, w, in the latter. In these expressions, a is the segment length. For a good solvent neither the ν dependence nor the exponent is reliable due to a breakdown of the mean-field approach, but for the Θ solvent the self-consistent calculation should be reasonably accurate.[12] The front factor in eq 5 determines the prefactor ρ in eq 2, which therefore depends on w (and on a).

In this paper we study adsorbed homopolymer under Θ conditions. To control the polymer density, we vary the coefficient ρ of $P(L)$ and identify the interaction parameter w to which this corresponds (e.g., by numerically matching the segment density profile). The power law distributions given above are, of course, cut off by the maximum loop size which is on the order of the contour length of the adsorbed polymers. We say more about the cutoff chosen in section 3. The following model for the loop layer is now made: (1) We consider each loop to be a Gaussian random walk starting and ending at the same point on the surface. This is appropriate under Θ conditions, but might also be used to describe polymers in good solvent, provided the loop distribution is adjusted to reflect the correct density profile. (2) Although the loops are anchored at the surface, they can pass through the surface from one side to the other. Statically, this does not really matter as long as the prefactor (and perhaps the cutoff) of the loop size distribution is adjusted to maintain the correct density profile. Dynamically, the situation is less clear, but since (as shown below) the chain segments that lie on the adsorbing plane are essentially frozen, the two-sided problem studied here should be almost equivalent to a one-sided one. (In fact, the statistics for a one-sided Gaussian random walk can be implemented, but are computationally more cumbersome.) (3) The constraint that the loop ends contact the surface at the same point could also be relaxed, for example, to model surface migration or adsorption/desorption kinetics, but these effects are ignored for our simplified calculations.

3. Dynamics

We now present an analysis of the dynamics of anchored loops, along the lines laid down by Freed and Edwards[7] for chains in solution. Formally these problems only differ in their specifications for the correlations both between monomers (on a given chain) and

also between chains. The first effect (arising because we have loops rather than open chains) is easily handled, whereas the second is more profound. The chain−chain correlations in the adsorbed loop problem violate translational invariance, and this is why we will have to resort to a numerical calculation (section 3c). Throughout the following, we take units where $k_BT = 1$ and the Gaussian step length is $a = (3/2)^{1/2}$.

In the Freed−Edwards formalism, which describes the dynamics of Gaussian chains with hydrodynamic interactions, the strategy is as follows: (a) Couple chains to solvent with a no-slip boundary condition. (b) For a given polymer configuration, calculate the associated thermodynamic force on each chain and (by Newton's third law) the reaction force on the fluid. (c) Calculate the perturbation to the velocity field arising from this force. (d) Then use the no-slip boundary condition to obtain a dynamical equation for the polymer motion in terms of the perturbed fluid motion, and preaverage. (The result of this is essentially the Zimm equation for the polymer dynamics.) Using this equation, (e) eliminate the polymer motion from the velocity perturbation (this involves summing over all polymers present) and (f) express this perturbation as a renormalization of the Oseen hydrodynamic propagator. In the conventional Freed−Edwards theory, this renormalized propagator is translationally invariant, and a frequency-dependent dynamic viscosity can be directly read from it. In our work, we proceed through (a)−(e), but the renormalized propagator explicitly involves the position of the adsorbed layer. Nonetheless, it may be used to compute the mean flow field in the presence of the polymer.

3.a. A Single Anchored Polymer Loop under Flow. Consider first the spatial path of a loop, $\mathbf{R}(s)$ (with $\mathbf{R}$ a spatial vector and s, with $0 \le s \le L$, a monomer index). We may write

$$\mathbf{R}(s) = \sum_n \mathbf{R}_q \sin qs \tag{6}$$

where $\mathbf{R}_q$ is the Fourier amplitude corresponding to the nth Rouse/Zimm mode of the loop ($q = n\pi/L$; $n = 1, 2, ...$). (Modifications appropriate for tails are detailed in section 3d.) The local stretching of the polymer exerts a thermodynamic (entropic) force density, $\sigma(\mathbf{r})$, on the fluid,

$$\sigma(\mathbf{r}) = \int_0^L \mathrm{d}s\, \delta[\mathbf{r} - \mathbf{R}(s)][\partial^2\mathbf{R}(s)/\partial s^2] \tag{7}$$

or, in a shorthand notation, by

$$\sigma(\mathbf{r}) = \psi D\mathbf{R} \tag{8}$$

where

$$\psi = \int_0^L \mathrm{d}s\, \psi_s \tag{9}$$

is the integral of the density operator, defined as

$$\psi_s = \delta[\mathbf{r} - \mathbf{R}(s)] \tag{10}$$

and

$$D = \partial^2/\partial s^2 \tag{11}$$

The force field σ is a reaction force on the fluid, which must be present since an entropic force per unit length, $-D\mathbf{R}(s)$, is needed on the polymer to maintain a deformed shape.[12,13]

The response of a bulk fluid medium to any force exerted upon it (by the polymer or externally) is governed by a hydrodynamic propagator, $\mathbf{G}_0$, which we take to be the usual Oseen tensor

$$\mathbf{G}_0(\mathbf{r}) = \frac{1}{8\pi\eta_s}\frac{\mathbf{I} + \hat{\mathbf{r}}\hat{\mathbf{r}}}{|r|} \tag{12}$$

In fact, for the adsorbed layer problem, this is a deliberate simplification. The true hydrodynamic propagator, in the presence of a stationary wall, requires an additional image source term to match the boundary conditions, and is therefore more complicated than eq 12. However, as discussed previously, we expect that the high polymer density at the surface will act to screen out hydrodynamic interactions that penetrate from one side of the wall to the other. Thus, when the polymer is included, the final, renormalized, fluid propagator will obey the required boundary condition even if the bare one does not. Since we are only interested in the properties of the final system, it does not matter if we start from a model where the adsorbing surface (without polymer) is transparent to flow. We will test our assumption later (section 4a) by monitoring the leakage of flow through the polymer layer.

Given our specification for $\mathbf{G}_0$, if $\mathbf{u}_0$ is the bare flow in the absence of polymer, we have

$$\mathbf{u}_0(\mathbf{r}) = \int \mathrm{d}^3\mathbf{r}'\, \mathbf{G}_0(\mathbf{r}-\mathbf{r}')\, \mathbf{F}(\mathbf{r}') \equiv \mathbf{G}_0\cdot\mathbf{F} \tag{13}$$

where from now on we use the compact notation ($\cdot$) to represent a real-space convolution. In this equation, $\mathbf{F}$ represents the bare force density acting on the fluid. This force includes external forces, such as that exerted by a distant plate moving to produce shear flow, and also Langevin random forces (which will generally be ignored in what follows). Equation 13 does not include the forces arising from the distorted polymer configurations. The presence of polymer introduces an additional force field, σ, obeying eq 8, and modifies the flow to be

$$\mathbf{u} = \mathbf{G}_0\cdot\mathbf{F} + \mathbf{G}_0\cdot\psi D\mathbf{R} \tag{14}$$

Next, we impose no-slip boundary conditions everywhere on the polymer; that is to say, the polymer is embedded in, and travels with, the fluid. This constraint can be written compactly as

$$\dot{\mathbf{R}}(s) = \psi_s\cdot\mathbf{u}$$

Introducing the Fourier-space density operator

$$\hat{\psi}_q = (2/L)\int_0^L \mathrm{d}s\, (\sin qs)\psi_s \tag{15}$$

we obtain an equation of motion for the polymer, as follows:

$$\dot{\mathbf{R}}_q = \hat{\psi}_q\cdot\mathbf{u} = \hat{\psi}_q\cdot\mathbf{G}_0\cdot\mathbf{F} + \hat{\psi}_q\cdot\mathbf{G}_0\cdot\psi D\mathbf{R} \tag{16}$$

The last term on the right represents the influence of a thermodynamic force, associated with distortion of the polymer at one point in space, on the velocity of a section of polymer at another point in space. Within a Zimm-level approximation, we can preaverage the hydrodynamic propagator using the probability distribution for polymer conformations. After preaveraging, we expect the hydrodynamic propagator to be nearly diagonal in

the Rouse modes,[13] and we can write

$$\dot{\mathbf{R}}_q = \hat{\psi}_q \cdot \mathbf{G}_0 \cdot \mathbf{F} - (L/2) q^2 G_0(q) \mathbf{R}_q \tag{17}$$

where $G_0(q) = \langle \hat{\psi}_q \cdot \mathbf{G}_0 \cdot \hat{\psi}_q \rangle$, with the angular brackets denoting an average over polymer configurations, and we have identified, in q space,

$$D = -q^2 \tag{18}$$

which follows from eq 11. The average above is taken over the distorted polymer distribution under flow. To linear order in the flow, however, the average can be taken over the equilibrium static polymer distribution; an exact form is given below.

For a specified preaveraged $\mathbf{G}_0$, the dynamical mode amplitudes of the polymer can then be written compactly as

$$\mathbf{R}_q = G_q \hat{\psi}_q \cdot \mathbf{G}_0 \cdot \mathbf{F} \tag{19}$$

where G_q is the polymer Green's function given by

$$G_q = [i\omega + (L/2) q^2 G_0(q)]^{-1} \tag{20}$$

In writing the equations above, we have made use of the linearity of eq 17 in implicitly writing all dynamical quantities in terms of their components at an imposed frequency, ω.

So far, we have eqs 19 and 20 which describe the reaction of the polymer to an external force, $\mathbf{F}$, where the response function is inversely related to the configurational average of the hydrodynamic propagator between two points on the polymer. The next step is to calculate the flow field $\mathbf{u}$ arising from $\mathbf{F}$; because of the polymer, this differs from the bare flow $\mathbf{u}_0 = \mathbf{G}_0 \cdot \mathbf{F}$. In the presence of one polymer with configuration $\mathbf{R}_q$, the flow profile becomes

$$\mathbf{u} = \mathbf{G}_0 \cdot \mathbf{F} + \mathbf{G}_0 \cdot \sum_n \langle \hat{\psi}_q D G_q \hat{\psi}_q \rangle \cdot \mathbf{G}_0 \cdot \mathbf{F} = [\mathbf{G}_0 - \mathbf{G}_0 \cdot \mathbf{T} \cdot \mathbf{G}_0] \cdot \mathbf{F} \tag{21}$$

where we can identify $\mathbf{T}$ as a "scattering" kernel, given by (recall $q = n\pi/L$)

$$\mathbf{T}(\mathbf{r},\mathbf{r}') = -\sum_{n=1}^{n_{\max}} \langle \hat{\psi}_q(\mathbf{r}) D G_q \hat{\psi}_q(\mathbf{r}') \rangle = \sum_n \frac{\langle \hat{\psi}_q(\mathbf{r})\, \hat{\psi}_q(\mathbf{r}') \rangle}{(2i\omega/Lq^2) + G_0(q)} \tag{22}$$

Note that, in the case of static ($\omega \to 0$) flow, $\mathbf{T}$ takes the particularly simple form

$$\mathbf{T}(\mathbf{r},\mathbf{r}') = \sum_n \frac{\langle \hat{\psi}_q(\mathbf{r})\, \hat{\psi}_q(\mathbf{r}') \rangle}{G_0(q)} \tag{23}$$

The upper cutoff in the summation is taken at $n_{\max}(L) = \max[1, [L/a]]$ corresponding to a fixed cutoff length, $q_{\max}^{-1}$, at the size of the smallest loops ($\simeq a$).

The full nonlinear solution of the combined polymer and flow distortions then involves summing the scattering from many chains (see below) and finding the self-consistent solution of the above equations. In particular, the averaged hydrodynamic propagator $G_0(q)$ as well as $\mathbf{T}$ needs to be evaluated for a chain distorted by the flow field. The flow field is itself, however, determined from this distorted $G_0(q)$ as it enters $\mathbf{T}$. (Note that a self-consistent iteration is required even though hydrodynamic screening effects are neglected.)

Rather than attempt this task, in the rest of this paper we will consider only the change in the flow field to linear order in shear rate, which involves eqs 21 and 22, where the angular brackets from now on represent averages taken over the *zero-flow* equilibrium polymer distribution. In this case, the preaveraged hydrodynamic interaction can be found exactly. Indeed, for a loop anchored at the origin (that is, a point on the adsorbing plane which—we recall—the loop is free to cross) the equilibrium monomer-ordered two-point correlation function for the polymer is

$$\rho_{ss'}(\mathbf{r},\mathbf{r}') = \left[\frac{L}{\pi^2 s(L-s')(s'-s)}\right]^{3/2} \times \exp\left\{-\left[\frac{\mathbf{r}^2}{s} + \frac{\mathbf{r}'^2}{L-s'} + \frac{(\mathbf{r}'-\mathbf{r})^2}{s'-s}\right]\right\} \quad \text{for} \quad s < s' \tag{24}$$

and the averaged propagator $G_0(q)$ can be evaluated as

$$G_0(q) = c_0 \left(\frac{2}{L}\right)^2 \int_0^L \int_0^L \mathrm{d}s\, \mathrm{d}s' \sin(qs) \sin(qs') \times \int\int \mathrm{d}\mathbf{r}\, \mathrm{d}\mathbf{r}'\, \rho_{ss'}(\mathbf{r},\mathbf{r}')/|\mathbf{r}-\mathbf{r}'|$$

$$= (-1)^{n/2} 4 c_0 \left(\frac{6}{\pi L}\right)^{1/2} \left[\frac{\pi}{2} J_0(n\pi/2)\right] \quad \text{for even } n \tag{25}$$

$$= (-1)^{(n-1)/2} 4 c_0 \left(\frac{6}{\pi L}\right)^{1/2} \left[\frac{1}{n} J_0(n\pi/2) + \pi 2 J_1(n\pi/2)\right] \quad \text{for odd } n$$

where the numerical prefactor c_0 has the value $1/(6\pi\eta_s)$, which has absorbed the factor of 4/3 for isotropic averaging of the Oseen tensor in eq 12. The asymptotic expansion of the Bessel functions gives $G_0(q) \approx n^{-1/2} + O(n^{-3/2})$. This expansion (when the prefactor is included) is quite accurate for even values of n (less than 5% error); for $n = 1$, it is about half the exact value while for other odd values of n it differs by less than 25%. For our numerical work, however, we use the exact expression above.

3.b. Many Loops of Different Sizes. We consider now the case of an adsorbed homopolymer layer under Θ conditions. As previously described, we build a model of the adsorbed layer out of Gaussian loops. In that case, the blob structure has the familiar self-similar geometry, in which loops of a given size are marginally overlapping. We may then expect that, in this marginally correlated regime, the contributions from the hydrodynamic scattering of many loops will tend to be dominated by sequences of statistically uncorrelated polymer loops. More specifically, if $\mathbf{T}_L$ is the scattering kernel from a loop of contour length L, and $P(L)$ is the number of such loops per unit surface area, then we can define a single-scattering kernel as

$$\bar{\mathbf{T}} = \int \mathrm{d}L\, P(L) \mathbf{T}_L \tag{26}$$

and consider the total perturbation on the flow to be the result of all uncorrelated sequences of hydrodynamic

scatterings from different polymer loops, i.e.

$$\langle \mathbf{u} \rangle = [\mathbf{G}_0 - \mathbf{G}_0 \cdot \bar{\mathbf{T}} \cdot \mathbf{G}_0 + \mathbf{G}_0 \cdot \bar{\mathbf{T}} \cdot \mathbf{G}_0 \cdot \bar{\mathbf{T}} \cdot \mathbf{G}_0 - \ldots] \cdot \mathbf{F}$$
$$= [\mathbf{I} + \mathbf{G}_0 \cdot \bar{\mathbf{T}}]^{-1} \cdot \mathbf{u}_0 \quad (27)$$

This approximation corresponds to a Zimm-model calculation of the viscosity, as performed in ref 7a. Therefore, it does not allow for any hydrodynamic screening effects.[7b] We believe their omission to be appropriate because of the marginal overlap condition. However, we cannot exclude the possibility that a self-consistent treatment of screening would alter our results. The situation is rather similar to that found for the hydrodynamics of cross-linked fractal objects close to the gelation threshold: in that system, too, there is a marginal overlap condition[14] and the role of screening in the system remains controversial. In fact, it would be very simple to solve our equations in the (extreme) opposite limit of pure Rouse dynamics. However, in such a model one recovers a local friction which is certainly not accurate in the outer parts of the layer, where the polymer density is very low. A full calculation with partial screening might be interesting, but is beyond our present scope.

3.c. Calculation Method. Although the scattering from a single anchored polymer is localized near the anchoring point in the adsorbing plane, the total scattering kernel from a layer obeys translational invariance in the transverse direction. This leads to a simplification which we now describe. Of major interest is the case where the external term **F** represents distant planes of force, chosen to give a uniform shear flow in the absence of polymer, that is, $\mathbf{u}_0(z) = u_0(z)\hat{\mathbf{x}}$, where z is a coordinate normal to the adsorbing surface and x and y are parallel ones; u_0 is linear in z. In this case, only the $k_x = k_y = 0$ components of $\bar{\mathbf{T}}$ and $\mathbf{G}_0$ need be retained: in a partial Fourier transform (transverse direction only) we have for the Oseen propagator

$$\mathbf{G}_0(\mathbf{r})_{k_x=k_y=0} = (1/2\eta_s)(-|z| + D)\hat{z}\hat{z} \quad (28)$$

Here the large finite constant D (discussed below) is proportional to the linear dimension of the plane of force and $\bar{\mathbf{T}}_{k_x=k_y=0}$ depends on the z-projection of $\rho_{ss'}(\mathbf{r},\mathbf{r}')$, which is

$$\rho_{ss'}(z,z') = \left[\frac{L}{\pi^2 s(L-s')(s'-s)}\right]^{1/2} \times \exp\left\{-\left[\frac{z^2}{s} + \frac{z'^2}{L-s'} + \frac{(z'-z)^2}{s'-s}\right]\right\} \quad \text{for} \quad s < s' \quad (29)$$

In our numerical work, we start from eq 27, which determines the perturbed flow field $\langle \mathbf{u} \rangle = [\mathbf{I} + \mathbf{G}_0 \cdot \bar{\mathbf{T}}]^{-1} \cdot \mathbf{u}_0$ (below we drop the angled brackets) in terms of the unperturbed flow $\mathbf{u}_0$. In practice, we first compute the operator $\mathbf{G}_0 \cdot \mathbf{T}$ as follows: we analytically perform the convolution of $\mathbf{G}_0(\mathbf{r})_{k_x=k_y=0}$ with $\rho_{ss'}(z,z')$ and then numerically take the 2-D Fourier transform on s, s'. Dividing by $\langle \hat{\psi}_q \cdot \mathbf{G}_0 \cdot \hat{\psi}_q \rangle$, and summing over q modes, gives, according to eq 23, $\mathbf{G}_0 \cdot \mathbf{T}(z,z')$ as required. The 2-D sine transform is actually evaluated in terms of 1-D fast Fourier transform (FFT) cosine transforms since only diagonal terms are needed. To find **u**, we first average $\mathbf{G}_0 \cdot \mathbf{T}$ over the chain size distribution to get $\mathbf{G}_0 \cdot \bar{\mathbf{T}}$, and then construct the operator $[\mathbf{I} + \mathbf{G}_0 \cdot \bar{\mathbf{T}}]$ as a matrix on a discretized z, z' grid. Typically 50 grid points are used, although we have also performed checks for convergence with changes in the grid spacing. This matrix is then inverted, and the real space convolution with $\mathbf{u}_0$ finally evaluated, by matrix multiplication, to determine $\mathbf{u}(z)$.

Care must be taken in dealing with the large finite constant D in $\mathbf{G}_0$. In fact, in a geometry where the flow is antisymmetric about the polymer plane, such as a two-sided shear problem, D cancels exactly from the final results, and can be set to zero. For confined symmetric flows, such as Poiseuille flow between parallel plates, the constraining boundary forces again cancel any dependence of the results on the value of the constant D. The details of the handling of this constant in the hydrodynamic propagator are provided in the Appendix.

Otherwise, the main numerical subtleties are connected with issues of convergence in the mode sum for **T**, eq 22. In particular, the FFT needs to be corrected to be accurate to $O(N^{-2})$, where N is the number of discrete samples, as an approximation for the continuous cosine transform in the domain $0 \le s \le L$. Otherwise, the errors on the order of $O(N^{-1})$ arising from the standard discrete FFT (which in effect performs a rectangular sum approximation to the integral) accumulate in the mode sum to produce a spurious order unity error. To achieve the required degree of accuracy, we make the equivalent of a trapezoidal approximation:

$$\int_0^L \mathrm{d}s \cos(qs) f(s) \approx \left(\frac{L}{N}\right)\left\{\sum_{m=0}^{N-1} \cos\left(\frac{mn\pi}{N}\right) f\left(\frac{mL}{N}\right) + \frac{1}{2}[\cos(n\pi) f(L) - f(0)]\right\} \quad (30)$$

where the first term on the right-hand side is evaluated using a traditional discrete cosine FFT. With this scheme for performing the cosine transform, we find good convergence using 512 modes, although for the larger loops we use more. Furthermore, we have checked the mode convergence against analytical results available in the low-density perturbative limit, which we discuss below. It is found (both analytically and numerically) in this limit that the mode sum for **T** converges as $N^{-1/2}$; by comparing prefactors against the analytical results, we estimate that using $n_{\max} = 512$ modes we are, for steady flows, less than 5% away from the $n_{\max} \to \infty$ limit.

3.d. Inclusion of Tails. The effect of tails can be included by minor changes in our formalism, as long as the length distribution for tails is specified along with that for the loops. The fact that one end of a tail is free, and the other bound to the surface, alters the boundary conditions of the Rouse/Zimm modes; this can be accounted for by changing the q-values of the modes from $n\pi/L$ to $(n - 1/2)\pi/L$. In addition, the two-point monomer correlation function is modified; it becomes

$$\rho_{ss'}(\mathbf{r},\mathbf{r}') = \left[\frac{1}{\pi^2 s(s'-s)}\right]^{3/2} \times \exp\left\{-\left[\frac{\mathbf{r}^2}{s} + \frac{(\mathbf{r}'-\mathbf{r})^2}{s'-s}\right]\right\} \quad \text{for} \quad s < s' \quad (31)$$

which also implies that the hydrodynamic matrix ele-

ment $G_0(q)$ is altered to

$$G_0(q) = 4c\left(\frac{6}{\pi L}\right)^{1/2}\left\{\frac{2}{(2n+1)^{1/2}}C[(2n+1)^{1/2}] + \frac{2}{\pi(2n+1)^{3/2}}S[(2n+1)^{1/2}] + \frac{(-1)^{n+1}}{\pi n}\right\} \quad (32)$$

where $C(x)$ and $S(x)$ are the Fresnel cosine and sine integrals, respectively. The expression above for tails is in fact numerically fairly close to that for loops, differing by less than 30% for all values of n. It is thought[15] that the tails extend from the wall to distances on the order of the size of the polymer, and can therefore be hydrodynamically active at the same level as the largest loops. However, there are only two tails per chain, and many loops, so the inner part of the layer is not much affected. Although to include tails would entail only trivial adjustments to the formalism, it is not clear what proportion of tails, and what size distribution, is appropriate: this should depend on the molecular weight of the adsorbed chains. (Once tails and loops are both present, the information cannot be inferred from the segment density profile directly, as in eq 2.) For comparison we have done some trial calculations with tails, and discuss these at the end of section 4a.

4. Flow near a Single Layer

We now present numerical calculations for the flow field **u** in the presence of adsorbed homopolymer under Θ conditions. (As stated in section 2, this corresponds to a value of $\tau = 2$ for the loop size distribution exponent.) Unless otherwise stated, we choose a value of $\rho = 10$ (corresponding to a value of $w \approx 0.002$) for the three-body interaction parameter, as values of $\rho = 1$ (i.e., $w \approx 0.2$) to $\rho = 10$ correspond to a range of typical coverages for marginal overlap between the smallest loops. (However, we also study the w dependence in detail below.) For all our calculations, we use a "squared" discretization of the loop distribution: $L = i^2$, with $i = 1, 2, 3,...$ To account for the finite maximum length of the loops in the distal regime, we impose a sharp cutoff at L_c on the loop size distribution $P(L)$. In fact, we have also tried an exponential cutoff of the form

$$P(L) = \rho L^{-2} \exp(L/L_c) \quad (33)$$

with $L_c = 100$ and further absolute cutoffs at $L_{max} = 529$ and $L_{min} = 1$, but the results remain qualitatively equivalent. For the sharp cutoff and exponential cutoff alike, the prefactor ρ of the loop size distribution can be directly related to w by a matching of the density profile. The data presented below are for a sharp cutoff at $L_c = 23^2 = 529$, unless otherwise stated.

4.a. Steady Shear Flow. We first present calculations for the case of constant gradient shear flow, as perturbed by the presence of polymer adsorbed to the $z = 0$ plane. We consider a two-sided problem in which the flow is antisymmetric about $z = 0$ for the flow profiles (with the polymer density symmetric); our graphs only depict the flow for positive z. Since linear response is assumed, the scale of the velocity is fixed by the asymptotic shear gradient associated with $\mathbf{u}_0$; we take this arbitrarily to be unity in the plots.

Convergence with Mode Number. Plots for several values of n_{max}, the number of q modes counted for the largest loops, are shown in Figure 1 to illustrate the degree of convergence. Results are plotted on linear (Figure 1a) and logarithmic (Figure 1b) axes. As stated above, a value of $\rho = 10$ is used. It is notable that the slope of the plot in the inner region is characterized by an exponent, y (defined by $u(z) \approx z^y$), which is close to 2.0, and independent of the mode cutoff when this is large. This result, which is also independent of w as shown below, appears robust. Moreover, the amplitude of the power law is expected to be well converged by $n_{max} = 512$ modes, as is supported by the fact that the $n_{max} = 128$ and $n_{max} = 512$ curves are nearly indistinguishable on the scale of the graph. Figure 2 illustrates the dependence of the hydrodynamic thickness (which is the z intercept of the far-field asympotote to $u(z)$) on the mode number for the same parameters. We have assumed the convergence to a presumed limiting value proceeds as a power law (as is known to be the case in the perturbative low coverage limit), and have fit our results accordingly. We find a value of $R_H \approx 9.46a$ in the limit of $n_{max} \to \infty$, with convergence scaling as $n_{max}^{-0.67}$ (illustrated in the plot by a best linear fit to the data).

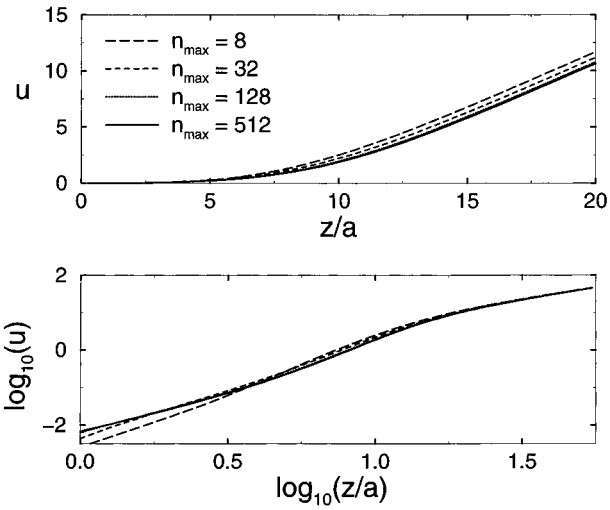

Figure 1. (a, top) Fluid velocity **u**(z) in an adsorbed polymer layer placed in a steady shear field. The layer coverage is given by $\rho = 10$ and the upper loop cutoff $L_c = 529$. Plots for values for $n_{max} = 8$, 32, 128, and 512, the number of q modes used, are shown to illustrate convergence, with $n_{max} = 128$ and $n_{max} = 512$ nearly indistinguishable on the scale of the figure. (b, bottom) The same on logarithmic axes. Again, $n_{max} = 128$ and $n_{max} = 512$ are nearly indistinguishable.

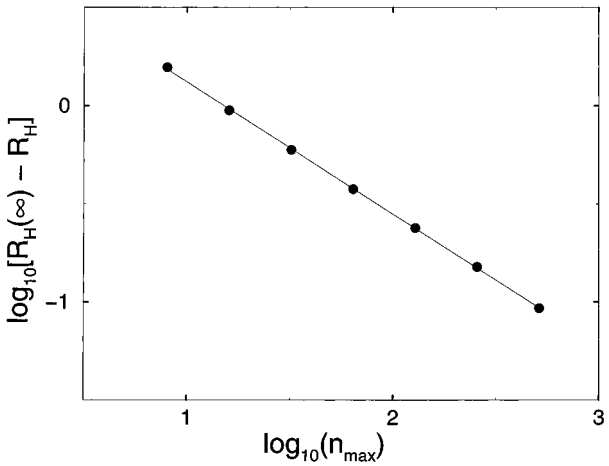

Figure 2. Convergence of the hydrodynamic thickness, R_H, with n_{max} to an extrapolated $n_{max} \to \infty$ limiting value of $R_H(\infty) = 9.46a$. The line is a best linear fit to the differences from $R_H(\infty)$, and has a slope of ~ -0.67. Results are for the layer corresponding to Figure 1.

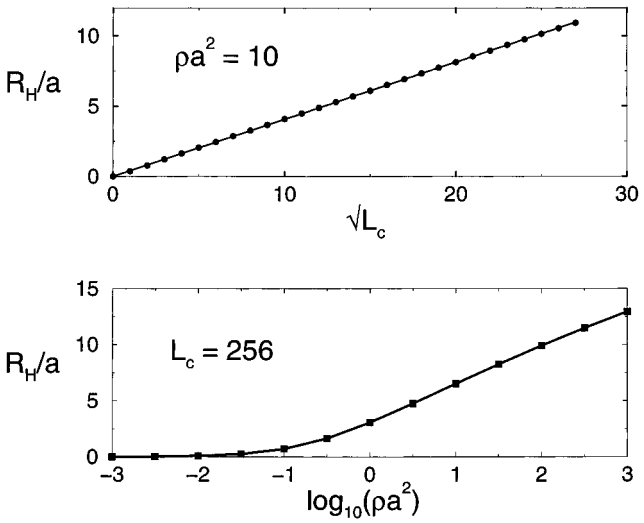

Figure 3. Dependence of the hydrodynamic thickness R_H on (a, top) the loop size cutoff L_c and (b, bottom) the areal density ρ.

In the perturbative limit, the response is dominated by single scattering, and so we can write the hydrodynamic radius simply as

$$R_H = \frac{1}{\dot\gamma}[u_0(\infty) - u(\infty)] = G_0(\infty,z')\cdot\bar{T}\cdot u_0/\dot\gamma = \frac{3}{4(2\pi)^{1/2}}\int P(L)L^{3/2}\sum_n n^{-3/2} \quad (34)$$

The convergence of the sum as $n^{-1/2}$ for a given loop size, L, has been verified numerically (along with the prefactor), serving as a further check of the convergence with mode number.

Hydrodynamic Thickness. On physical grounds[10] we expect at fixed w the magnitude of R_H to be controlled by the spatial extent of the largest loops, which is on the order of $L_c^{1/2}$. Figure 3a illustrates the linear relationship between R_H and $L_c^{1/2}$. Plots at other values of ρ yield equally good linear fits. The scaling seems satisfactory, and any departure from linearity should arise mainly from discretization error, or finite grid effects at large values of R_H. In addition, we find good $L_c^{1/2}$ scaling for the entire velocity profile, including the inner region, and not just for R_H, as illustrated for two values of L_c in Figure 4. This is another strong indication that our steady-shear results are fully converged. More interesting is the dependence of R_H on the interaction parameter w, or equivalently the loop density parameter ρ. Figure 3b shows the result (we choose $L_c = 256$): the hydrodynamic radius, though scaling correctly with L_c as just described, has a residual weak dependence on ρ. The data suggest that this could be logarithmic. It appears that within our approach the hydrodynamic thickness may increase indefinitely with ρ; although at first alarming, this may not be too unreasonable since it does not take much polymer to immobilize the fluid and (for Gaussian loops) there is always some small polymer density extending to infinity away from the wall (arising from chains that happen to be strongly stretched). Crudely, one might argue that R_H is defined by the point where the polymer density drops below some small fixed value, in which case one would have, for large ρ, the scaling $R_H \approx (\ln \rho)^{1/2}$. The data are more consistent with a simple logarithmic dependence.

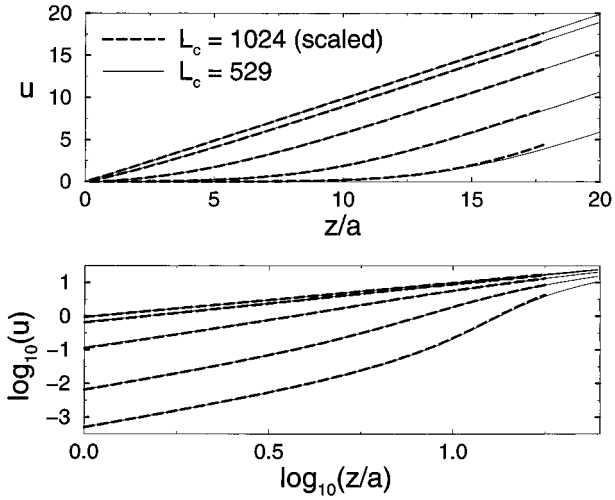

Figure 4. Scaling of the fluid velocity profiles with the loop cutoff L_c shown on (a, top) linear axes and (b, bottom) logarithmic axes. Plots are given for values of $\rho = 0.01$, 0.1, 1, 10, and 100. The data for $L_c = 1024$ (heavy dashed line) has been rescaled by a factor of $(529/1024)^{1/2}$ to illustrate scaling with the $L_c = 529$ data (thin solid line).

Flow Profile near the Wall. The effect of varying the density is more strongly detectable in the velocity profile near the wall than in R_H. Parts a and b of Figure 5 show $u(z)$ against z on log and linear axes, respectively, for various values of ρ. These data show that as ρ is increased the flow velocity near the wall is supressed, which is expected. More surprising is that the asymptotic slope of the log plot at small z is apparently independent of ρ. (This breaks down only at the very lowest densities; we guess that for these the asymptotic power law regime may still be present, but at z values that are too small to be probed with the present discretization.) Assuming this power to be ρ independent, the best estimate of it can be obtained by including large ρ data for which the scaling region is relatively wide. (Data for ρ up to 1000 are shown.) Our best estimate of the exponent y found in this way is

$$y = 2.0 \pm 0.1 \quad (35)$$

Note that this exponent does not depend on the mode number cutoff, as shown previously.

Since $\bar{\mathbf{T}}$ is linear in ρ, the apparent universality of the exponent y suggests that, to calculate the flow in the inner region, the operator $[\mathbf{I} + \mathbf{G}_0\cdot\bar{\mathbf{T}}]$ appearing in the equation

$$\mathbf{u} = [\mathbf{I} + \mathbf{G}_0\cdot\bar{\mathbf{T}}]^{-1}\cdot\mathbf{u}_0$$

might be approximated by neglecting the unit operator $\mathbf{I}$. If this is the case, one recovers a simple scaling: at fixed z,

$$u(z) \propto 1/\rho \quad (36)$$

This is found numerically to be true, as shown in Figure 6.

A Universal Scaling Behavior? The exponent y was found above to be independent of the mode cutoff and also independent of the physical density of the layer. An important physical question is whether this exponent and also the scaling eq 36 are universal properties of adsorbed polymer layers (at the Θ point), or whether they vary with the chemical or other details of the system.[5] We have therefore performed careful

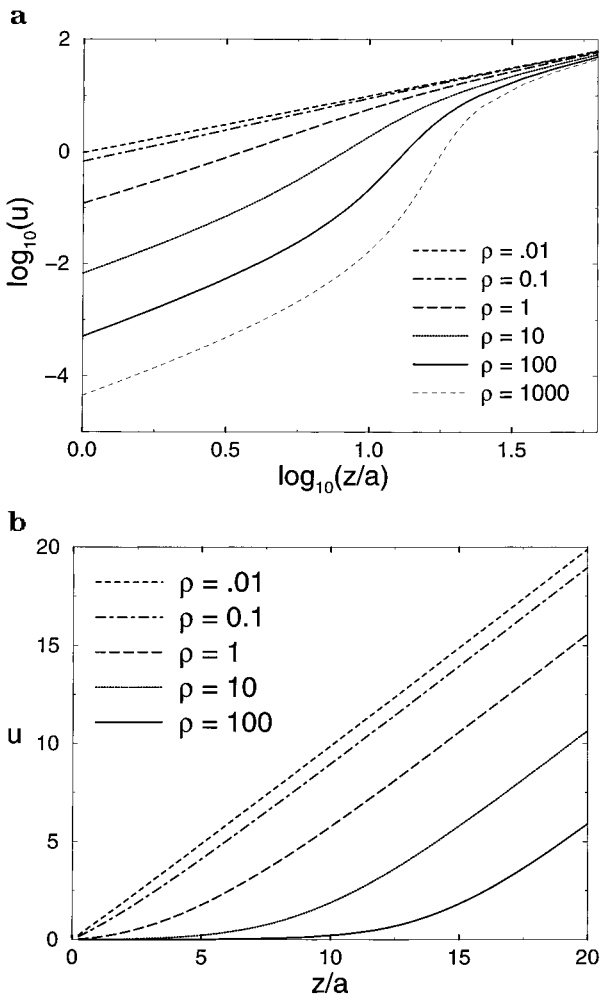

Figure 5. Flow profiles (with $L_c = 529$) for a range of $\rho = 0.01$, 0.1, 1, 10, 100, and 1000 on (a, top) logarithmic and (b, bottom) linear axes. Data for $\rho = 1000$ are not shown in the linear plot. From the logarithmic plot, one finds for the near-wall profile the exponent $y = 2.0 \pm 0.1$ apparently independent of ρ (for $\rho > 0.1$).

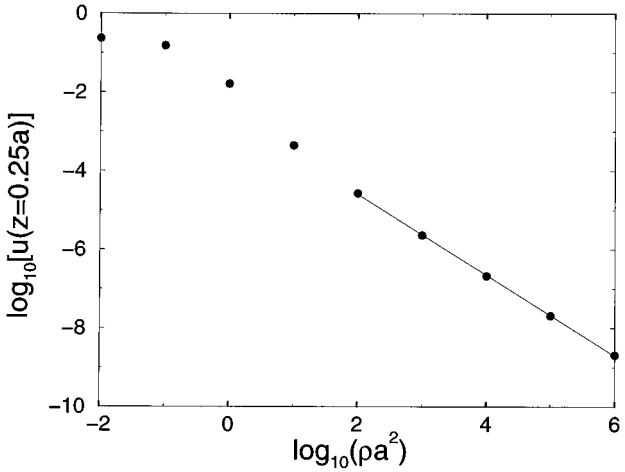

Figure 6. log−log plot of the near-wall velocity profile $u(z)$, sampled at $z = 0.25a$, versus ρ. The line is a best linear fit, found to have nearly unit slope, verifying the large ρ scaling of the near-wall profile $u(z) \propto 1/\rho$.

checks of the robustness of the above findings by, for example, altering $\bar{T}$ by doubling the contribution of the first mode in the sum given by eq 23. We find that the exponent y is raised somewhat, to an effective value of ~2.5, though there is residual curvature in the plots which suggests that they might not be in the asymptotic

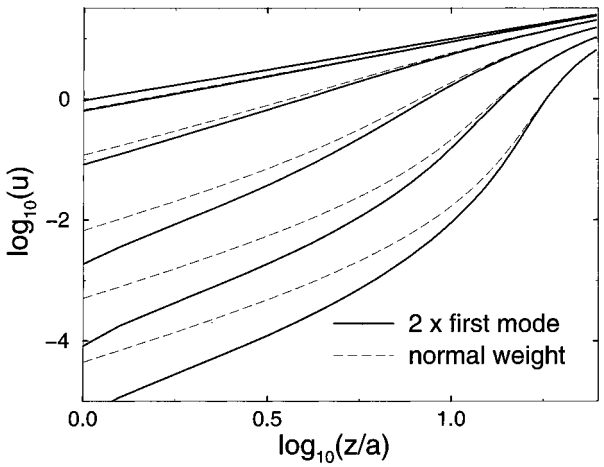

Figure 7. log−log plot of the flow profile when the first mode counts twice in the mode sum for $\bar{T}$ in eq 23 (heavy solid line). For comparison, the flow profile for correct (single) weighting of the first mode is displayed as the thin dashed line.

region. On the other hand, we still observe the scaling for $u(z)$ with respect to ρ in the inner region. This is shown in Figure 7. The apparent influence on y is similar to one found below on replacing the adsorbed layer of loops by one made entirely of tails with the same overall density profile. These sensitivities could indicate that the exponent y is not, in fact, universal, or it could be that y is universal in reality, but that its calculated value depends on some (though not all) of the details of the model. We return to this point at the end of the paper.

Role of Wall Permeability. As stated in section 1, we expect our flow predictions to be unaffected by whether the adsorbing wall is penetrable to fluid. This is because an initially transparent wall becomes impenetrable when coated with polymer (whose segment density is very large at the wall). If this is correct, then we would expect that the effects of fluid flow or forces exerted on one side of the wall to be undetectable from the other side. To check this, we took the case of a bare flow, $\mathbf{u}_0(z)$, which is linear shear for one side and zero for the other side. (However, to compensate for the long-ranged force on a moving infinite slab, we closed the flow far away into an antisymmetric back-flowing loop.) The profile for such a flow ($\rho = 10$ and $L_c = 529$) is shown in Figure 8. The polymer-induced modification of a one-sided linear shear field, u_0, for $z > 0$ is similar to that arising for a two-sided flow (shown as the dashed line). (The discontinuities at $\pm 10a$ are artifacts associated with the coincident discontinuities in the hydrodynamic forces associated with the bare flow.) This test confirms that the flow profile on one side of $z = 0$ is independent of what happens on the other; i.e., the wall is effectively impenetrable to fluid. We have also performed another check of the hydrodynamic screening between the two sides separated by the polymer layer by adding a "wall" in the form of a layer at $z = 0$ consisting of a huge number of small loops. Results for a 1000-fold increase above the normal abundance of small ($L = a$) loops are shown in Figure 9, confirming our claim that results derived using the two-sided hydrodynamic propagator are equivalent, within discretization error, to that obtained for the one-sided problem accounting for the hydrodynamic effects of a solid wall.

Comparison with Darcy-Type Local Porosity Models. Previous models of steady flow through a layer

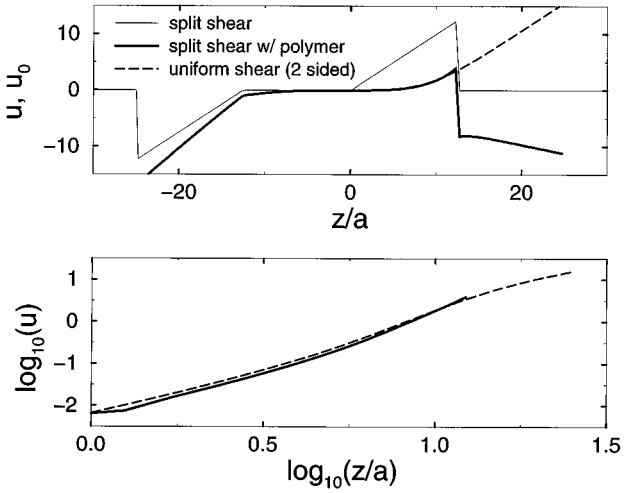

Figure 8. Polymer layer subjected to a one-sided (split) shear flow. (a, top) Flow profiles are shown in the absence (thin solid line) and presence (heavy solid line) of polymer. The dashed line is the flow profile for the two-sided shear used in previous plots (shown for positive z only). (b, bottom) log−log plot of flow in a polymer layer placed in one-sided (heavy solid line) and two-sided (dashed line) shear.

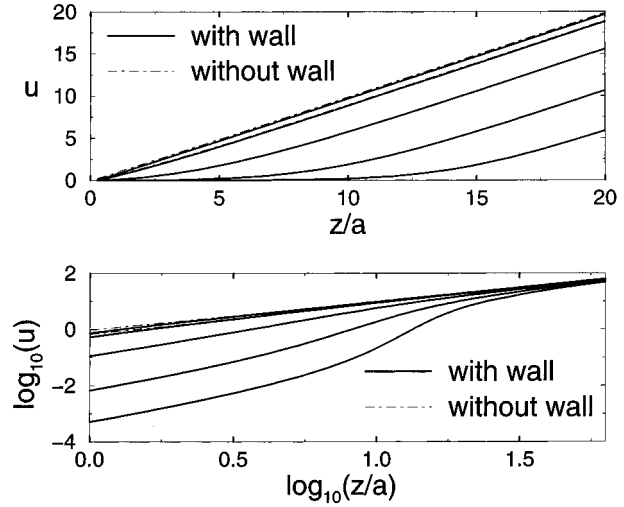

Figure 9. Flow in the presence of an additional "wall", composed of 1000 times the normal abundance of tiny ($L = 1$) loops placed at $z = 0$. For comparison, profiles are also shown (thin dotted−dashed line) in the absence of the wall. Plots for (a, top) linear and (b, bottom) logarithmic axes show that, even without an explicit wall, the flow on one side is hydrodynamically screened from the other side by the existing smallest loops.

of adsorbed polymer characterize the polymer as a static porous medium.[10,16] Depending on the assumed geometry of the loops (e.g., independent segments, rods, or coils), different functional forms for the effective local friction, $f(\phi)$, can be adopted. The resulting effect on linear shear flow through such a static medium can then be determined from the Debye−Brinkman equation

$$d^2u/dz^2 - f(\phi)u = 0 \tag{37}$$

which can be derived as a specific case of eq 27 by making the association $\mathbf{G}_0^{-1} \propto \partial_z^2$, and restricting the scattering kernel to be local, i.e., $T(\mathbf{r},\mathbf{r}') \propto f(\phi(\mathbf{r}))\,\delta(\mathbf{r}-\mathbf{r}')$. One form for the local friction which has been used[16] is the semiempirical fit

$$f(\phi) = \kappa_1 \frac{\phi}{1 - c\phi} \tag{38}$$

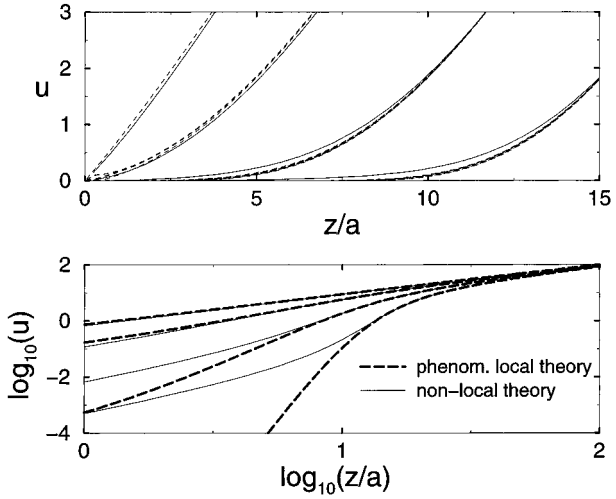

Figure 10. Comparison of the flow profiles $u(z)$ as predicted by the current nonlocal theory (thin solid lines) with those of the semiempirical porous medium theory of ref 16 (dashed lines), when fit to the same value of R_H. Data are shown for $\rho = 0.1$, 1, 10, and 100 and $L_c = 529$. (a, top) The plot on linear axes shows several values of the cooperative drag parameter $c = 0$, 0.1, 0.2, 0.3, 0.4, and 0.5, which are nearly indistinguishable. (b, bottom) The logarithmic plot shows good agreement for low values of $\rho \leq 1$, but greatly reduced flows for the local theory for $\rho = 10$ and $\rho = 100$. Only curves for $c = 0$ are shown.

which gives a linear dependence on ϕ at low densities, corresponding to a local segment friction, and the denominator is meant to correct for many-body cooperative drag effects at higher densities. Here κ_1 and c are phenomenological constants. A second choice has been the dependence $f(\phi) \approx \xi(z)^{-2}$, associated with drag through a "mesh" of characteristic length $\xi(z)$. For a self-similar adsorbed layer, this results in the form

$$f(\phi) = \kappa_2\phi^2 \tag{39}$$

which in the asymptotic scaling limit ($\xi(z) \approx z$) can also be written as $f(z) = \kappa_3 z^{-2}$. The parameter κ_2 controls the magnitude of the friction; within the scaling approach to polymers its magnitude is unknown[10] (though a value on the order of unity is expected). Note that in terms of κ_3 one has $y(y - 1) = \kappa_3$;[10] thus, if y is a universal exponent, then κ_3 is a universal constant. Conversely, insofar as κ_3 depends on the density, ρ (which within a mean-field description it certainly does), the model predicts a nonuniversal value of y. In any case, no simple machinery exists to calculate κ_3.

With either of these local models, the density profile, which is directly determinable for the distribution of loops (including cutoffs and discretization) used in our calculations, can be input to determine numerically the local friction f and hence the flow profile using eq 37. (This is a somewhat fairer comparison than using directly the asymptotic form for the density, eq 5.) In Figures 10 and 11, we compare the predicted flow profiles of our method (using $L_c = 529$ and $n_{max} = 512$) with these local porosity methods. To eliminate the unknown κ parameters, we demand that the hydrodynamic thicknesses agree with our own results. This then allows the *shapes* of the flow profiles to be compared in a parameter-independent way.

For the semiempirical model, eq 38, we find that the parameter c does not have a great effect on the flow profile, once a value of R_H has been picked. Thus, the six values of $c = 0$, 0.1, 0.2, 0.3, 0.4, and 0.5 plotted as

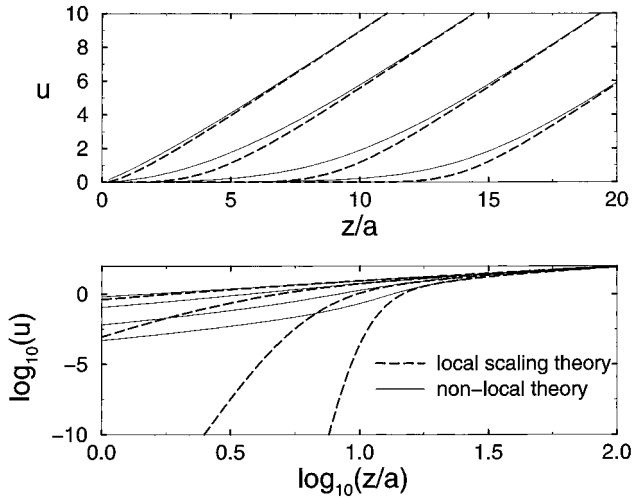

Figure 11. Comparison of the flow profiles $u(z)$ as predicted by the current nonlocal theory (thin solid lines) with those of the scaling porous "mesh" theory of ref 10 (heavy dashed lines), when fit to the same value of R_H. Data are shown for $\rho = 0.1$, 1, 10, and 100 and $L_c = 529$ on (a, top) linear and (b, bottom) logarithmic axes. Note the extremely reduced flows for the scaling theory near the wall as compared to those for the nonlocal theory.

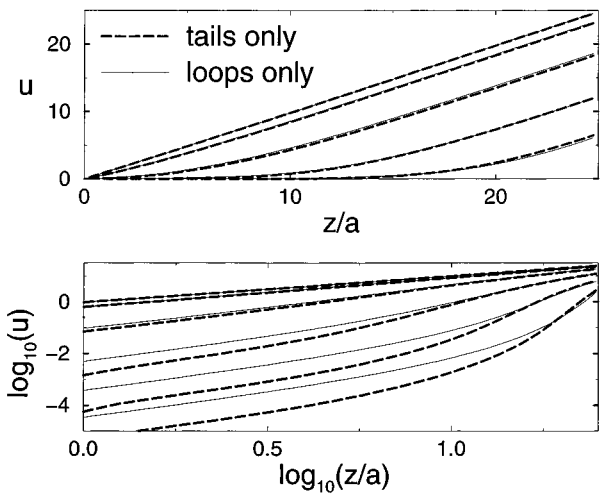

Figure 12. Comparison of a layer composed of tails ($L_c = 1024$; heavy dashed line) and a layer of loops ($L_c = 256$; thin solid line). Shown are flow profiles for $\rho = 0.01$, 0.1, 1, 10, and 100. On linear axes (a, top), it can be seen that tails produce a hydrodynamic thickness roughly twice that from loops of the same mass. On logarithmic axes (b, bottom), it can be seen that the near-wall profile decays with a slightly higher exponent for tails than for loops.

the dashed curves in Figure 10a are nearly coincident. As can be seen, the flow profiles from our nonlocal model can be fit more closely with the semiempirical form (using a single value of κ_1) than with the scaling theory discussed below, particularly for small $\rho \leq 1$. For the plots of $\rho = 10$ and 100, however, the semiempirical local model, like the scaling theory, gives flow velocities near the wall that are much smaller than our new predictions. Moreover, the behavior near the wall is not a power law (unless $c = 0$), as can be confirmed directly from eq 37, in contrast to our own findings. (In Figure 10b, we only show plots for $c = 0$, which gives the best overall match for a single value of c.) Contrary to our own preliminary results, as previously reported,[5] the fit values of κ_1 were not found to vary dramatically with ρ: for the data shown in Figure 10, κ_1 varies between 0.67 and 0.81.

Within the scaling theory, eq 39, if we match R_H for a given density profile, we find very small flow velocities near the wall, with extremely large values of the exponent y compared to our own predictions. This is illustrated in Figure 11. In particular, the values of $\kappa_3 \simeq 10^3$ deduced from these values of y are unexpectedly large. The values of κ_2 used to calculate the profiles, while smaller, are still somewhat large: they range from $\kappa_2 = 460$ for $\rho = 0.01$ to about $\kappa_2 = 18$ for $\rho = 1000$. Conversely, if one were to choose a local scaling theory with $\kappa_3 \simeq 2$, the hydrodynamic thickness for a given density profile would be much smaller than our own. Furthermore, in any consistent local description, this parameter should certainly be constant, and not ρ-dependent as found from our fits.

In summary, both of these local porous medium theories give predictions very different from our own, especially for the flow in the inner region, near the wall. These comparisons, of course, do not say directly which of the three theories is preferable. However, it is clear that our nonlocal approach yields results that qualitatively differ from those of earlier, local models.

Flow Profile As Given by Streaming Potential Measurements. The hydrodynamic thickness, which can easily be determined by experiment, is only a somewhat coarse measure of our predicted flow profiles: it does not probe the structure of the flow within the layer. In principle, streaming potential measurements[17] can be used to probe the flow in these regions. Specifically, by a careful enough experiment, it should be possible to extract an estimate of the wall flow exponent y. In streaming potential experiments, polymers are adsorbed onto a charged wall and the potential gradient along the wall is measured in the presence of an adjacent fluid flow. The width λ of the counterion double layer at the adsorbing surface is controlled by the salt concentration. In the absence of a potential gradient, the fluid flow would convect a current of counterions, I, obeying

$$I \propto \int_0^\infty dz\, e^{-z/\lambda} u(z) \tag{40}$$

where λ is the Debye length. To maintain charge neutrality, a potential difference, $V \propto I$, must be set up. Thus, in an idealized measurement, the streaming potential is related directly to the Laplace transform of the flow velocity profile, and is very sensitive to the near-wall behavior. Unfortunately,[17] these experiments are difficult, and it is not at present feasible to Laplace invert the experimental data in order to extract an estimate for y.

Role of Tails. To allow a more direct comparison of the hydrodynamic activity of tails to loops, we first considered the hypothetical case of an equivalent self-similar adsorbed layer of tails (as if all loops released one of their contacts to produce a tail). In doing so, the same loop mass extends a greater distance into the solvent. Since we know that only a small amount of polymer is necessary to perturb surrounding fluid, we can make an estimate of the proportional effect of replacing a loop by a tail of equal mass by considering the extension of the farthest monomer into the solvent. A simple calculation shows that the far end of the tail protrudes twice as far as does the monomer halfway around a loop from the anchoring monomer. In fact a comparison of the flow profiles for a layer of loops with $L_c = 1024$, and a layer of tails with a quarter the length ($L_c = 256$), shown in Figure 12, confirms that this simple

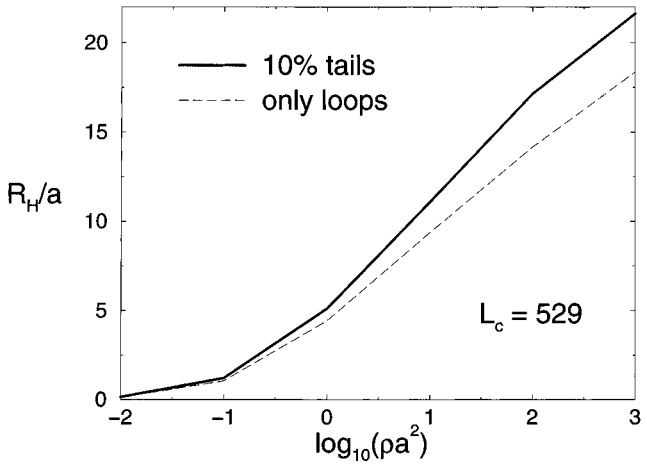

Figure 13. Effect of tails on the hydrodynamic thickness, R_H. Plotted are curves for a layer of loops as discussed in this paper ($L_c = 529$, shown as the thin dashed line), and a layer where 10% of the loops have been converted to tails (heavy solid line). For the range displayed, the effect of tails is to increase R_H by about 15−20%.

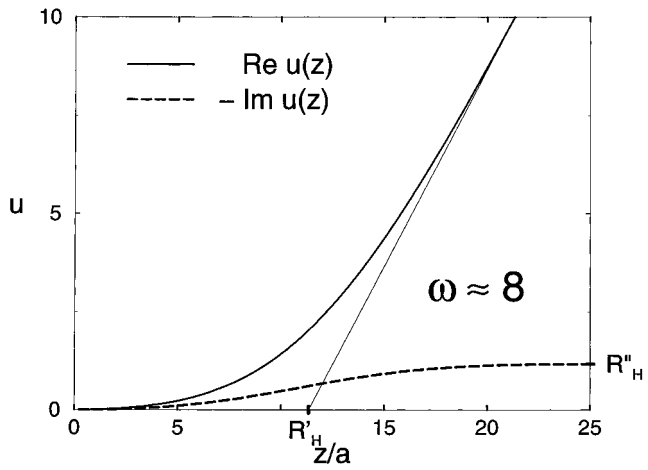

Figure 14. Real (heavy solid) and (negative) imaginary (heavy dashed) parts of the complex flow profile $u(z)$ in an adsorbed polymer layer ($L_c = 1024$, $n_{max} = 1024$, $\rho = 10$) subjected to oscillatory shear with frequency $\omega = 8.36$. Indicated intercepts are the real (R_H') and imaginary (R_H'') parts of the complex hydrodynamic thickness R_H^*.

argument is fairly accurate. Near the anchoring point, however, the differing chain statistics between a singly and doubly anchored polymer apparently are important. In particular, they alter the exponent y to a value of approximately $y \approx 2.5$ for a layer of pure tails. In any real layer composed of both loops and tails, the loop density will predominate near the wall, and hence the loop-only value for the exponent y should prevail.

In any case, in the outer region, a low density of longer tails can produce a noticeable change in the hydrodynamic radius. As a rough estimate of the effect of the presence of a minority of tails in an adsorbed layer, we have calculated the velocity profiles for a layer consisting of 90% loops and 10% tails, both obeying the same power law decomposition. (This greatly overestimates the number of small tails, but this should not matter far from the wall.) Figure 13 plots R_H for both the mixed loop−tail layer and the pure loop layer, using $L_c = 529$ for both, for a range of ρ values. Over the range $\rho = 0.01-1000$, the effect of tails is to increase the hydrodynamic thickness by about 15−20%.

4.b. Oscillatory Shear. We now turn to a discussion of finite frequency effects, again restricting ourselves to the case of shear flow near a single adsorbed layer. We can use the existing formalism of section 3 (which includes the frequency ω as a parameter) to study the in- and out-of-phase velocity patterns within the layer in response to an oscillatory far-field force. The finite relaxation time of the polymers leads to a viscoelastic behavior which can be quantified in various ways. Here we choose to describe it in terms of a complex hydrodynamic thickness.[5] Sens et al.[18] have recently addressed the same issues from a qualitative (scaling) perspective; these authors prefer to use a complex elastic modulus.

We choose time units so that τ_{max}, the longest (Zimm) relaxation time of the largest loops, is unity. In terms of previously defined quantities, we have

$$\tau_{max} = 3(2\pi)^{1/2} L^{3/2} (\eta_s / k_B T) \qquad (41)$$

Figure 14 shows results for the (complex) flow profile for a polymer layer with $L_c = 1024$ and $n_{max} = 1024$, subjected to oscillatory flow at frequency $\omega = 8.36$. Note the out-of-phase (i.e., elastic) response, arising from the inner region. The intercepts shown on the figure

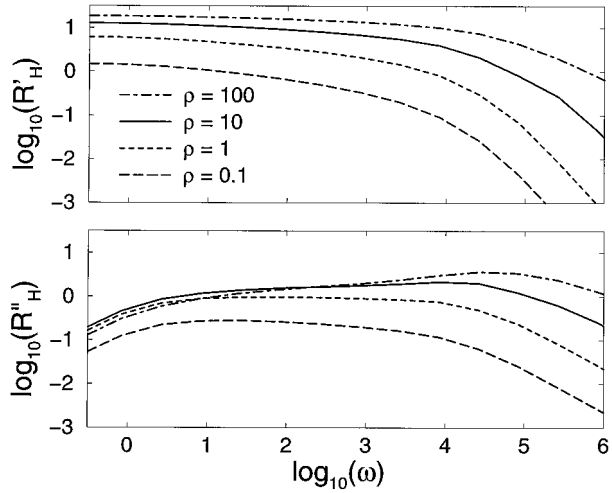

Figure 15. Complex hydrodynamic thickness, R_H^*, for the layer corresponding to Figure 14 ($L_c = 1024$). The top panel shows the real part, R_H', decreasing with ω, while the bottom panel shows the nonmonotonic behavior of the imaginary part.

correspond to the real and imaginary parts of a complex hydrodynamic thickness, $R_H^*(\omega)$, as we now describe.

Consider a plate held at a distance, L, far from the (fixed) adsorbing surface, on which is exerted a tangential force, F, per unit area. In the absence of polymer, the velocity of this plate is $u_0 = FL$ (in units where the solvent viscosity $\eta_s = 1$). In steady shear, the polymer modifies this far-field velocity to $u = F(L - R_H)$; hence, $(L - R_H)^{-1}$ can be identified as the mechanical (velocity) impedance of the system. Continuing this to finite frequency ω defines the complex hydrodynamic thickness $R_H^*(\omega) = R_H'(\omega) + iR_H''(\omega)$. In the far-field region ($L \gg R_H$) the amplitude of the oscillatory flow response is $|u| = F(L - R_H'(\omega))$, while the phase shift is given by $\arg(u) = R_H''(\omega)/L$.

Figure 15 shows results for $R_H^*(\omega)$, for density parameters $\rho = 0.1$, 1, 10, and 100. While $R_H'(\omega)$ decreases modestly until frequencies on the order of τ_{min}^{-1} are reached, $R_H''(\omega)$ shows an intermediate regime for $\tau_{max}^{-1} < \omega < \tau_{min}^{-1}$. The ratio R_H''/R_H' shows a rising trend in this region as an increasing number of modes contribute to the elastic part of the response. On general grounds, one expects a ratio on the order of

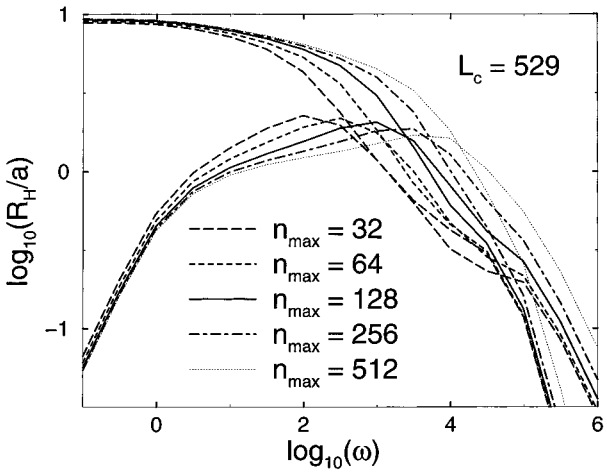

Figure 16. Real and imaginary parts of the complex hydrodynamic thickness, R_H^*, for various values of the upper mode cutoff, $n_{max} = 32, 64, 128, 256, 512$.

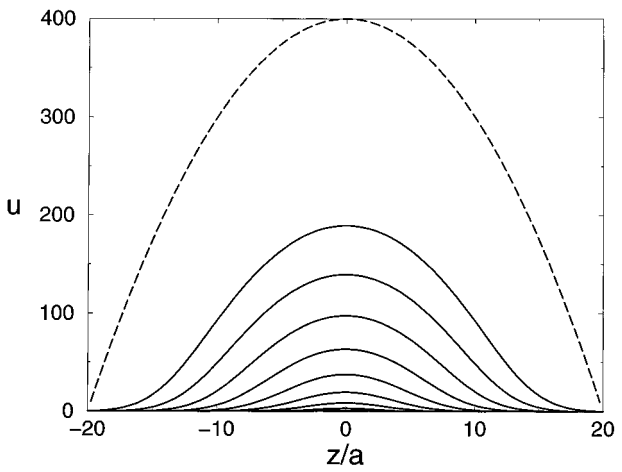

Figure 17. Fluid velocity between parallel plates with adsorbed polymer, at various interplate separations, $h/a = 40, 36, 32, 28, \ldots$ Also shown is the parabolic flow between plates without adsorbed polymer at a separation of $h = 40a$ (dashed line). Note that $L_c = 256$ and $\rho = 10$ for each layer; in the shear geometry a single such layer produced a value of $R_H = 6.5a$.

unity for frequencies close to τ_{max}^{-1}, although the value found here is somewhat less (in the range 0.1−0.2). Figure 16 shows the effects of varying the mode cutoff on these results for a given value of the density parameter, $\rho = 10$ (i.e., $w \approx 0.002$). The mode cutoff has a strong effect at high frequencies but not at low ones. At lower values of n_{max}, a shoulder remains visible in R_H^* up to $\omega_{max} \approx 5$, before a final drop at higher ω. This residual response up to ω_{max} is due to contributions from loops of length smaller than L_c/n_{max}, for which we have chosen to assign $n_{max} = 1$ (one mode responding) rather than $n_{max} = 0$ (no response whatsoever).

These results might be tested, for example, in the standard force-machine setup in either the lateral oscillation mode or the axial compression mode (under a lubrication flow approximation).[19] At first sight, our findings, particularly for R_H'', contradict the scaling arguments of Sens et al.,[18] who predict at high frequency a decaying power law with frequency for both the real and imaginary part of the hydrodynamic thickness, $R_H \approx (i\omega)^{-1/3}$. It may be that for the mode numbers and loop lengths used here we cannot expect to reach a clean high frequency asymptote, as addressed by the scaling theory, before effects from the upper frequency cutoff (the Zimm time of the shortest loops) come into play. However, we see no clear indication in the log plot (Figure 15) of an emerging power law.

It is interesting, in any case, that the hydrodynamic thickness, or at least its real part, is a decreasing function of frequency. This contrasts, at first sight, with the physical view of polymers as becoming more and more immobile at high frequency (hence, the elastic contribution). However, this is balanced by an effect whereby the polymers immobilize smaller and smaller amounts of solvent as ω is increased: the imposed frequency defines a characteristic length scale beyond which the polymers become effectively transparent to flow. This idea, which is the basis of the scaling theory,[18] can also be used to understand the high-frequency rheology of free chains in solution.[13] The complex elastic modulus of such a solution is an increasing function of frequency ($G^*(\omega) \approx (i\omega)^{2/3}$), but this translates to a dynamic complex viscosity, $\eta^* = G^*/i\omega$ (and hence hydrodynamic radius of the coils), which is a decreasing function.

5. Flow between Two Plates

In this section we return to the case of steady flows, but consider the problem of two parallel adsorbed layers with a channel in between. In colloidal suspensions, two polymer-coated particles in collision will feel a squeeze force from a thin lubrication layer whose properties can be strongly altered by the presence of the polymer.[1] As a model of such lubrication flow, we consider the attenuation of a parabolic flow profile between two plates when polymer is adsorbed on both surfaces. For simplicity we treat the layers as simply overlapping; that is, we do not adjust the density profile in response to the presence of a second layer. The hydrodynamic scattering treatment includes scatterings from one layer to another, but as in the single layer case, screening contributions are omitted.

For uncoated surfaces, the flow is perfectly parabolic, and vanishes at the walls (located at $z = \pm h/2$):

$$u_0(z) = h^2/4 - z^2 \tag{42}$$

where a prefactor of unity has been chosen arbitrarily. The constraint of zero velocity at the walls is enforced by introducing wall forces which counteract the stresses arising from the flow between the plates. These forces are determined by requiring the fluid velocity to be zero outside the plates. Their magnitude is not fixed, but depends on the density and separation of the polymer layers; because of this, the solution of our equations is more complex for the two-layer system than a single layer. The extra constraint forces, in a real system, are supplied by the rigid walls and oppose the drag forces exerted on the polymer chains by the moving fluid. As discussed further in the Appendix, this constraint of zero fluid velocity outside the plates in fact again allows our calculation to proceed without having to prescribe a particular value of the parameter D appearing in the hydrodynamic propagator $\mathbf{G}_0$ (eq 28).

Figure 17 shows the attenuated flows in the presence of adsorbed polymer for different separations h between the plates. Each wall has a layer of adsorbed polymer with $L_c = 256$, $n_{max} = 256$, and $\rho = 10$; a single layer in the shear geometry was found (in the previous sections) to have a hydrodynamic thickness, R_H, of $6.5a$ (see Figure 3b). In all cases the unperturbed flow profile is given by eq 42. The parabolic flow in the absence of polymer is shown for the largest plate separation ($h =$

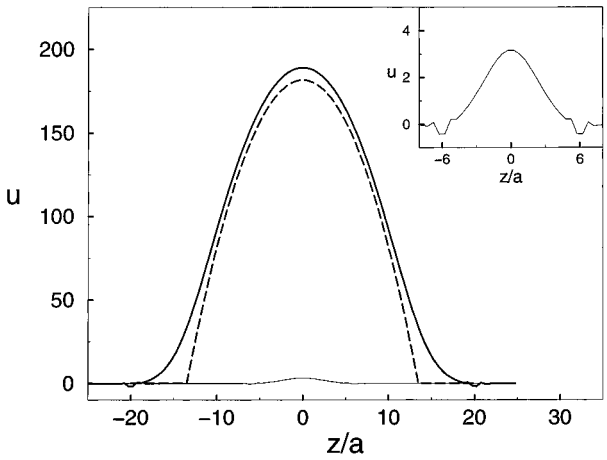

Figure 18. Flow profile for two plates separated by $h = 40a$ (same as in Figure 17; solid line), compared with the profile for two bare walls at separation $h - 2R_H$ (dashed line). The thin line (in main body of graph as well as magnification inset) shows the profile for plates with polymer separated by $h = 12a < 2R_H$. The rough bumps at the wall are numerical artifacts that decrease as the spatial grid is refined.

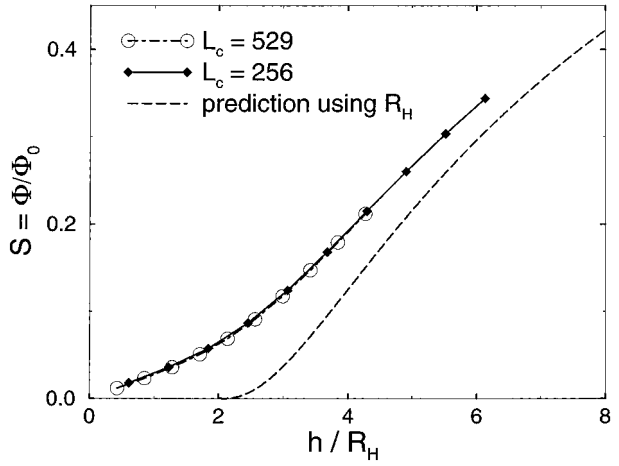

Figure 19. Blocking factor, S, defined as the ratio of the flux between plates with polymer to that without polymer, at various values of h/R_H. Data are shown for $L_c = 256$ and $L_c = 529$. The dashed line plots the blocking factor arising from completely impermeable layers of thickness R_H.

$40a$ or $h/R_H \approx 6.1$). Near the walls, the flow with polymer present exhibits a profile reminiscent of that in steady shear flow, while far from the walls between the plates, the parabolic shape of the flow is recovered, although at reduced velocities. At large separations, as expected, the effect of the polymer is therefore to displace inward the effective boundaries for the parabolic flow by a distance on the order of R_H for each polymer layer. This result, which becomes exact for large h/R_H, is confirmed in Figure 18, where the profile for $h = 40a$ is compared to the parabolic profile obtained by shifting each wall inward by the distance R_H. However, at smaller separations, the effect on the flow is more subtle; indeed, for $h < 2R_H$, one would formally predict zero flow at the level of a hydrodynamic thickness description. Of course the flow is not zero, and the residual permeability of the layer in the longitudinal direction is essentially a probe of the near-wall flow behavior. The inset in Figure 18 shows this weak flow (also shown for comparison in the main body of the figure) when the plates are spaced $h = 12a$ apart. The rough bumps at the wall boundary are numerical artifacts resulting from the strong discontinuities in force at the wall boundaries. These artifacts become smaller as the spatial grid spacing is made finer.

Figure 19 shows the "blocking factor" S as a function of h/R_H. This is defined as $S = \Phi/\Phi_0$, where Φ is the fluid flux between the plates and Φ_0 its unperturbed value; since the calculation of $\mathbf{u}$ involves the same external fluid forces as that of $\mathbf{u}_0$ (except, of course, for the constraint forces on the plates), this ratio of fluxes is taken at fixed pressure gradient. For $h \ll R_H$ the density profile of the polymers within each layer is modified, but the effect should not be much different from that of eliminating loops whose spatial size is larger than h (there are few of these compared to the number of smaller ones, so folding them back toward the surface has little effect on the inner region). If so, then a scaling argument for the flux can be made as follows. We know that, in the inner region for shear flow, $u(z)/u_0(z) \approx (z/R_H)^{y-1}$ (where any dependence on the density parameter ρ is suppressed; we suppose $\rho \simeq 1$). Assuming this formula still to hold in the parallel plate geometry suggests that the blocking factor should vary as $(h/R_H)^{y-1}$ for small values of h/R_H. For $y \simeq 2.0$ this is consistent with the data of Figure 19. Data from two values of L_c are shown; these fall onto a common curve when distances are scaled by R_H. The dashed line indicates the blocking factor S_0 arising from completely impermeable layers of thickness R_H; obviously the difference is very significant for $h/R_H < 2$ (when $S_0 = 0$), but it remains substantial up to about twice this separation.

6. Discussion and Conclusions

We have described in this paper a systematic treatment of fluid flow in adsorbed homopolymer layers (represented as a sequence of adsorbed loops) at the Θ point. As previously discussed, the statistics of such a layer do not differ greatly from those in a good solvent (in particular, chains of a given size marginally overlap in each case), and we believe our results offer a useful benchmark model for adsorbed layers in general. Various approximations have been made to render the multiple-scattering formalism useable for numerical work, which is nontrivial since the problem does not show three-dimensional translational invariance. For the same reason we have limited our attention to the regime of linear response.

Our results for static flows show the expected scaling of hydrodynamic thickness R_H with the size of the largest loops in the layer (fixed in reality by the size of the adsorbed chains themselves), though a residual (logarithmic) dependence on the overall density of adsorbed chains remains. We attribute this to the contribution of atypical chains which stretch further than average into the solution; for practical purposes this logarithmic dependence can almost certainly be ignored. We also found numerically a power-law exponent for flow near the wall with value $y \simeq 2.0 \pm 0.1$. The power is numerically independent of the density ρ of the adsorbed loops (a fact consistent with the scaling of the velocity with ρ^{-1}, which was also found); however, it may depend on the mathematical details of the model to some extent. In particular we showed that doubling the hydrodynamic scattering by the lowest Zimm mode of each loop increased the power y somewhat (although doubling the scattering from *all* the modes is equivalent to a density increase and would have no effect). A similar increase was found on replacing all the loops in the homopolymer layer by tails of the same overall size

(a procedure which also affects mainly the lowest modes of each chain). While neither of these changes have much plausibility as alternative models of the adsorbed layer, they do show a residual sensitivity in our model to the assumed chain geometry. For example, we have decomposed the layer into a power-law distribution of closed loops, free to cross the surface but anchored at a point. It is possible that a noncrossing constraint, or a relaxation of our constraint that the loops return to the origin (not merely the $z = 0$ plane), would give a similar modification to the scattering kernel and hence to the exponent y. The same applies to the inclusion of screening effects which should also modify the scattering at the level of order unity factors (not more, because of the marginal overlap condition). Despite these warnings, we reiterate that our prediction for the exponent y is the first to be based on anything more than pure guesswork. Whether y represents a truly universal exponent remains an open question until a complete theory is developed.

A true homopolymer layer contains not only loops, but also a small fraction of tails which may, however, dominate the behavior at large distances (i.e., they can influence R_H). Our formalism allows these to be incorporated as long as the tail length distribution is known alongside that for loops. The apportioning of polymer length between loops and tails is a delicate issue however,[2,20] and we confined ourselves in this paper to a few representative calculations.

We have used our formalism to study the flow of fluid through a narrow channel in which adsorbed layers are present on each surface, and found confirmation of the scaling prediction that the flux through the channel for a given pressure drop varies as $(h/R_H)^{y-1}$ for small values of h, the channel width (a regime in which naive use of the hydrodynamic thickness concept would give zero flow). This might provide a more direct experimental probe of the near-wall flow behavior than the alternative technique of streaming potential measurements which yield (in principle) the Laplace transform of the velocity profile.

We turn now to our finite-frequency predictions for the impedance response (complex hydrodynamic thickness) of an adsorbed layer. Here the interesting behavior is when $\omega\tau_{max}$ is large (with τ_{max} the longest Zimm time). Despite being able to probe several decades of frequency before reaching τ_{min}^{-1} (the response frequency of the highest modes), we have been unable to extract a power law from our data. We are therefore not able to test the recent prediction of Sens et al.[18] that the complex hydrodynamic thickness should scale as $R_H \approx (i\omega)^{-1/3}$. Our data show a clear decreasing trend in the real part (the layer becomes increasingly transparent to high-frequency flow), but no matching trend is seen in the imaginary part (elastic response) until the high-frequency cutoff is encountered. On the basis of our data, it seems that rather large values of $\omega\tau_{max}$ are needed before any scaling asymptote is reached.

Finally, we discuss the prospects for predicting the properties of adsorbed homopolymer layers under strong flows, in which the layer structure, as well as the flow, is significantly perturbed ($\dot{\gamma}\tau_{max} \gg 1$). As mentioned previously, our formalism could handle this case in principle, at the expense of an extra self-consistency iteration to calculate the deformed polymer profile. (This would assume that the anchor points of the loops remain fixed—which is by no means certain.) With present computational resources, and also because the underlying physics is poorly understood, it seems more profitable at present to pursue a qualitative, scaling approach to this nonlinear regime. Calculations along these lines for end-attached brushes have been presented recently;[11] similar studies for adsorbed homopolymers are in progress.[21] However, an important ingredient of the scaling theories is the idea that the innermost part of the layer is relatively unperturbed by flow. (This same idea forms the basis of Sens et al.'s scaling predictions for low-amplitude, high-frequency shear.[18]) The scaling approaches to nonlinear flows therefore require as input a model of the linear response behavior, such as the one provided in this paper.

Acknowledgment. We acknowledge support from Unilever, ICI, Schlumberger, and the Department of Trade and Industry (U.K.) under the Colloid Technology program. We thank R. C. Ball for valuable help in the early stages of the project and J. L. Harden, J.-F. Joanny, A. Lips, C. M. Marques, and R. Varoqui for helpful discussions.

Appendix: 1-D Hydrodynamic Propagator for Layers

As discussed above, due to translational invariance in the $x-y$ plane, it is only necessary to keep the $k_x = k_y = 0$ components of the fully 3-D quantities appearing in the hydrodynamic equations. However, for the Oseen tensor, an integration over a region in the $x-y$ plane (corresponding to a planar area of force producing shear flow or boundary forces) results in an additive constant contribution, D, that scales with the area of integration. In particular, we can write (using units such that $2\eta_s = 1$)

$$\mathbf{G}_0 = \mathbf{G} + D \tag{43}$$

where $\mathbf{G} = -|z - z'|$ and is independent of the area of integration (see eq 28). The operator returning the perturbed flow from the original flow in the absence of polymer is given by eq 27, and can be rewritten as

$$\mathbf{P}_0 = [\mathbf{I} + \mathbf{G}_0\cdot\bar{\mathbf{T}}]^{-1} = [\mathbf{I} + \mathbf{G}\cdot\bar{\mathbf{T}} + D\cdot\bar{\mathbf{T}}]^{-1}$$

$$= [\mathbf{I} + \mathbf{P}\cdot D\cdot\bar{\mathbf{T}}]^{-1}\cdot\mathbf{P}$$

$$= \{\mathbf{I} + D[\int \mathrm{d}\bar{z}'\ \mathbf{P}(z,\bar{z}')][\int \mathrm{d}\bar{z}\ \bar{\mathbf{T}}(\bar{z},z')]\}^{-1}\cdot\mathbf{P}$$

where $\mathbf{P} = [\mathbf{I} + \mathbf{G}\cdot\bar{\mathbf{T}}]^{-1}$. The integrals appearing in the last equation imply that the combination $\mathbf{P}\cdot D\cdot\bar{\mathbf{T}}$ is even in both coordinates. Convolution with an antisymmetric source then cancels this term to zero, leaving

$$\mathbf{P}_0\cdot u_0 = \mathbf{P}\cdot u_0 \tag{44}$$

confirming that the constant D projects to zero when convoluted with an antisymmetric source, such as two-sided shear flow.

For symmetric sources, such as those for parabolic flow, the cancellation is not automatic, and depends on the boundary forces cancelling the total integrated force, as we will now explain. The final fluid velocity can be written as

$$u = \mathbf{G}_0\cdot F_{tot} = \mathbf{G}_0\cdot[\mathbf{I} + \bar{\mathbf{T}}\cdot\mathbf{G}_0]^{-1}\cdot F_0 \tag{45}$$

where

$$F_0 = F_{press} + F_{wall} \tag{46}$$

includes the original uniform force due to the pressure gradient, F_{press}, as well as the to-be-determined boundary forces, $F_{wall} \propto \delta(z - h/2) + \delta(z + h/2)$, needed to constrain the fluid velocity to vanish outside of the plates. The total of all the final forces acting on the fluid, F_{tot}, can be decomposed as

$$F_{tot} = F_0 + F_{poly} \tag{47}$$

where F_{poly} is the scattered force off the polymer (which is localized near the walls).

Consider now the constraint that the flow be a constant outside of the local region of the polymer and walls. Symmetric sources will produce in the far field a fluid velocity

$$\begin{aligned} u(z) &= (1/2)[\mathbf{G}_0(z,z') + \mathbf{G}_0(z,-z')]\cdot F_{tot}(z') \\ &= (1/2)(-|z - z'| - |z + z'| + 2D)\cdot F_{tot}(z') \\ &\approx (-|z| + D)\int dz'\, F_{tot}(z') \end{aligned} \tag{48}$$

where the constant is seen to represent overall translational motion of the entire system due to any net integrated force (in the localized source region) multiplied by the area over which the force is applied. More significantly, a constant fluid velocity outside the region of the polymer-coated walls implies that F_{tot} has zero integrated strength. Since F_{poly} is in general nonzero, this means the magnitude of the original boundary force F_{wall} is reduced by an amount equal to the integrated polymer drag force. From eq 45 above, we can then write

$$\begin{aligned} F_0 &= [\mathbf{I} + \bar{\mathbf{T}}\cdot\mathbf{G} + \bar{\mathbf{T}}\cdot D]\cdot F_{tot} \\ &= [\mathbf{I} + \bar{\mathbf{T}}\cdot\mathbf{G}]\cdot F_{tot} \end{aligned} \tag{49}$$

and so

$$F_{tot} = [\mathbf{I} + \bar{\mathbf{T}}\cdot\mathbf{G}]^{-1}\cdot(F_{press} + F_{wall}) \tag{50}$$

Provided the term $[\mathbf{I} + \bar{\mathbf{T}}\cdot\mathbf{G}]^{-1}\cdot F_{wall}$ (the total scattered force off the polymers originating from F_{wall}) does not integrate to zero (which in general it will not), there is a unique value for the magnitude of F_{wall} that produces zero integrated strength for F_{tot}. Equation 50 then leads to the expression for the velocity profile

$$u = \mathbf{G}_0\cdot F_{tot} = \mathbf{G}\cdot F_{tot} \tag{51}$$

which is *independent* of the constant D. To conclude, the prescription is therefore to adjust the boundary forces to balance the net integrated strength of the polymer and pressure forces (and thereby set the velocity to zero outside the walls); having satisfied the conditions of this boundary force, the constant D has no effect on the final flow profiles.

References and Notes

(1) Russel, W. B.; Saville, D. A.; Schowalter, W. R. *Colloidal Dispersions*; Cambridge University Press: Cambridge, 1989.
(2) Fleer, G. J.; Cohen Stuart, M. A.; Scheutjens, J. M. H. M.; Cosgrove, T.; Vincent, B. *Polymers at Interfaces*; Chapman and Hall: New York, 1993.
(3) Brooks, J. T.; Cates, M. E. *Macromolecules* **1992**, *25*, 391.
(4) Lips, A.; Campbell, I. J.; Pelan, E. G.; In *Food Polymers, Gels and Colloids*; Dickinson, E., Ed.; Royal Society of Chemistry: London 1991; Special Publication 82.
(5) Wu, D. T.; Cates, M. E. *Phys. Rev. Lett.* **1993**, *71*, 4142.
(6) Wu, D. T.; Cates, M. E. *Colloids Surf. A* **1994**, *86*, 275.
(7) (a) Edwards, S. F.; Freed, K. F. *J. Chem. Phys.* **1974**, *61*, 1189. (b) Freed, K. F.; Edwards, S. F. *J. Chem. Phys.* **1974**, *61*, 3626.
(8) Zimm, B. H. *J. Chem. Phys.* **1956**, *24*, 269.
(9) Guiselin, O. *Europhys. Lett.* **1992**, *17*, 225. See also: de Gennes, P.-G. *C. R. Acad. Sci., Ser. II* **1982**, *294*, 1317.
(10) de Gennes, P.-G. *Macromolecules* **1981**, *14*, 1637; *Macromolecules* **1980**, *13*, 1069; *C. R. Acad. Sci.* **1983**, *297*, 883.
(11) Harden, J. L.; Cates, M. E. *J. Phys. II* **1995**, *5*, 1093, 1757.
(12) de Gennes, P.-G. *Scaling Concepts in Polymer Physics*; Cornell: Ithaca, NY, 1979.
(13) Doi, M.; Edwards, S. F. *The Theory of Polymer Dynamics*; Clarendon: Oxford, 1986.
(14) Cates, M. E. *J. Phys.* **1985**, *46*, 1059.
(15) Ploehn, H. J.; Russel, W. B. *Macromolecules* **1989**, *22*, 266. Scheutjens, J. M. H. M.; Fleer, G. J.; Cohen Stuart, M. A. *Colloids Surf.* **1986**, *21*, 285.
(16) Cohen Stuart, M. A.; Waajen, F. H. W. H.; Dukhin, S. S. *Colloid Polym. Sci.* **1984**, *262*, 423. Cohen Stuart, M. A.; Waajen, F. H. W. H.; Cosgrove, T.; Vincent, B.; Crowley, T. L. *Macromolecules* **1984**, *17*, 1825.
(17) Cohen Stuart, M. A.; Mulder, J. W. *Colloids Surf.* **1985**, *15*, 49.
(18) Sens, P.; Marques, C. M.; Joanny, J. F. *Macromolecules* **1994**, *27*, 3812.
(19) Pelletier, E.; Montfort, J. P.; Loubet, J. L.; Tonck, A.; Georges, J. M. *Macromolecules* **1995**, *28*, 1990.
(20) Johner, A.; Joanny, J. F.; Rubinstein, M. *Europhys. Lett.* **1993**, *22*, 591.
(21) Harden, J.; Aubouy, M.; Cates, M. E. Manuscript in preparation.

MA951845B